HOT-WIRE MEASUREMENTS OF INSTABILITY WAVES ON CONES AT MACH 6

AIAA Paper 2006-3054, presented at the 36th AIAA Fluid Dynamics Conference,
San Francisco, CA, June 2006

Shann J. Rufer* and Steven P. Schneider†
School of Aeronautics and Astronautics
Purdue University
West Lafayette, IN 47906

Hot wires were used in the Mach-6 tunnel to obtain mass flux profiles and to study the amplitude and growth of instability waves on 7° half-angle sharp and blunt (0.020-inch radius) cones. Measurements were taken at several stagnation pressures (45, 70, 90, and 125 psia) on each of the cones. The boundary layer thickness at convention noise was similar for the sharp and blunt cones, though it was noticed that for the same pressure and axial location the boundary layer on the sharp cone was slightly thinner than that on the blunt cone. The measurements taken with the hot wires were then compared to computations using the STABL code. These comparisons show good agreement both in the shape of the mass flux profiles and the value of mass flux at the edge of the boundary layer. Good agreement was also seen in the frequency of the second-mode instabilities at various pressures; the frequencies found experimentally were within 8% of those calculated by STABL for all cases. Hot wire measurements were also obtained on a sharp cone under quiet-flow conditions and though no instabilities were observed at 0° angle of attack, when placed at a 3° angle of attack, peaks in the spectra were observed at 130 kHz which could be attributed to instabilities.

INTRODUCTION

The process of transition is not completely understood, even after years of research. The study of transition in the hypersonic flow regime becomes important due to the effect of transition on separation, heat transfer, and other boundary layer parameters. Though transition location can often be determined, the disturbance mechanisms which cause transition and the relationship between instability and transition remain uncertain [2]. As discussed in Ref. [3], very few accurate experimental studies of instability-wave growth have been conducted in hypersonic flow and an even smaller number of these have been completed with calibrated instrumentation.

In hypersonic flow, there are four basic instability mechanisms which produce disturbance growth: (1) first mode, or Tollmien-Schlichting, (2) second mode, or Mack mode, (3) cross-flow, and (4) Görtler [2]. The second mode instabilities, the most unstable of the Mack modes, tend to become dominant in hypersonic flow on symmetric models without concave curvature [4]. The second mode instability tends to occur at high frequencies when the boundary layer is 'thin' and at low frequencies for 'thick' boundary layers [5] and is most amplified when it is axisymmetric [6].

*Research Assistant. Member, AIAA.
†Professor. Associate Fellow, AIAA.

Transition on Blunt Cones

In hypersonic flow it is important to have a blunt leading edge in order to control the heating of the nose region of the vehicle. The effects of bluntness can be experienced by the flow hundreds of nosetip radii downstream. The actual distance that the effects seem to propagate is dependent on the bluntness and freestream conditions [7]. Leading edge bluntness also influences viscous-inviscid interaction, flow separation, pressure and velocity distributions, skin friction, heat transfer, and other properties.

Boundary-layer transition occurs in a fluid flow as instabilities in the flow cause small disturbances to grow, which in turn causes the flow to shift (transition) from laminar to turbulent. Transition involves many uncertainties and is therefore a very complex problem to solve. To alleviate some of the complexity, many experiments have been conducted on hypersonic boundary layer transition. These experiments assess numerous parametric trends, such as the effects of Mach number, nosetip bluntness, and unit Reynolds number, as well as many others.

A layer of high specific entropy and strong entropy gradients in the gas outside the boundary layer, commonly referred to as an entropy layer, is introduced into the flow downstream of the blunt nose (see Figure 1). This layer is a region of high temperature, low-density gas created by the large entropy increase in the gas as it passes through the bow shock caused by the bluntness on the leading edge [8]. The thickness of this layer is a function of the bluntness on the leading edge of the vehicle [7]. The entropy layer is important because of its effect on the growth of the viscous layer. When bluntness causes an entropy layer to be introduced into the flow, the viscous layer changes and grows through interaction with the entropy layer [9]. These new entropy effects also promote changes of the flow properties in the boundary layer and introduce a velocity and pressure gradient at the outer edge of the boundary layer [7]. The variable entropy effects caused by nose bluntness are 'swallowed' by the boundary layer at a certain length (termed the swallowing length) downstream of the nose. This, in turn, changes the properties of the boundary layer and the point at which transition occurs [9].

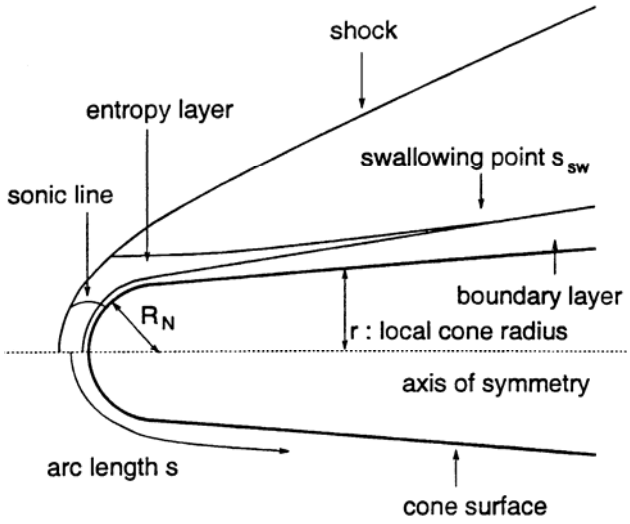

Figure 1 – A schematic diagram of supersonic flow over a blunt cone. From Ref. [11]

The effects of nose bluntness can be broken into two separate cases, those of 'small bluntness' and 'large bluntness' [10], [11]. In the small bluntness case, transition occurs near or behind the point where the entropy layer is swallowed by the boundary layer. For this case, the transition Reynolds number increases with increasing bluntness and the point of transition moves aft on the body. For the large bluntness case, where transition occurs well forward of the swallowing distance, the transition Reynolds number decreases rapidly with increasing bluntness and transition moves forward on the body. It was determined in Ref. [12] that in the case of small nosetip bluntness, increases in bluntness helped in the stabilization of the boundary layer.

It was shown in Ref. [5], through several transition experiments with nosetip radii of 0.15, 0.25, 0.5, and 0.7 inches, that a small bluntness on the vehicle nosetip can considerably increase the transition Reynolds number due to large increases in the critical Reynolds number (the Reynolds number beyond which the disturbances become unstable). For small nose radii (both 0.15 and 0.25 inches), the boundary layer appeared to be stable within the entropy-layer-swallowing region and the location of the critical Reynolds number seemed to coincide with the entropy-swallowing location, though the critical Reynolds number was not determined for the 0.25 inch radii nosetip. Ref. [13] states that the reason there is a stabilizing influence on the boundary layer is because "the effect of leading edge bluntness is to decrease the local Mach number, which would bring the boundary layer closer to separation, while at the same time lowering the local Reynolds number and increasing the favorable pressure gradient".

Effects of Angle of Attack on Transition

Though many experiments have been conducted on both sharp and blunt cones at zero and non-zero angles of attack, there is very little known about transition and the growth of instabilities on the leeward side of a blunt cone at non-zero angle of attack. It has been determined that with increasing angle of attack, the location of transition on the leeward side tends to move forward, though this effect seems to diminish as the angle of attack is increased further [14]. This forward motion of the transition location has been thought to be caused by the destabilizing effect of the cross flow [15]. The boundary layer on the leeward side of a cone is much thicker than that on a cone at zero angle of attack. On the windward side of a cone at angle of attack, the boundary layer thins. The thick leeward boundary layer causes the second mode disturbances to occur at much lower frequencies, similar in range to that of the first-mode instabilities seen on a sharp cone [5].

Measurements taken on the windward ray of a sharp cone at angle of attack have shown an increase in stability and a rearward movement of transition as compared to that of a cone at zero angle of attack [15]. The critical Reynolds number was found to increase on the windward ray as compared to a cone at zero angle of attack, though the growth rates of the second mode instabilities did not seem to be significantly affected [15]. The location of the onset of these disturbances, however, was greatly affected by the addition of an angle of attack [5]. It was also determined that the location of the onset of the disturbances on the leeward ray took place at a lower Reynolds number than that on a cone at zero angle of attack.

e^N Prediction Method

The e^N method is a semi-empirical method for predicting transition. The N-factor is the integrated growth-rate of an instability and can be calculated using

$$N(x) = \ln\left(\frac{A(x)}{A_0}\right),$$

where A(x) represents the disturbance amplitudes and A_0 is the amplitude at the point where the flow first becomes unstable at that frequency [11]. Stetson's experiments in AEDC Tunnel-B, a hypersonic conventional-noise tunnel, found an N-factor of about 5 at transition. This is significantly lower than the typical N-factor for flight conditions which has typical values between 9 and 10.

Boeing/Air Force Mach-6 Quiet-Flow Ludwieg Tube

The present study was conducted in the Purdue Mach-6 Quiet-Flow Ludwieg Tube. A Ludwieg Tube is similar to the more common shock tunnel. It consists mainly of a long pipe, or driver tube, a converging-diverging nozzle, and a set of burst diaphragms. The flow exits the nozzle into the test section and diffuser, which is connected to a large vacuum tank. The vacuum tank is separated from the pressurized upstream section of the tunnel by a set of diaphragms. When the differential pressure across the diaphragms becomes great enough, the diaphragms will burst. This causes a shock wave to travel downstream, into the vacuum tank, and an expansion wave to travel upstream, into the test section and driver tube, initiating hypersonic flow.

The Purdue Mach-6 Quiet-Flow Ludwieg Tube (see Figure 2 through Figure 4) operates on this principle. The driver tube is 17.5 inches in diameter and 122.5 feet long, and is connected to a tapered contraction section. A bleed slot is located near the end of the contraction section to bleed off the boundary layer before the flow enters the nozzle throat. The diaphragms are placed in the tunnel downstream of the test section and used to initiate the flow. Once the diaphragms have burst, there is, on average, a seven-second run before the pressure ratio is insufficient and the flow drops subsonic.

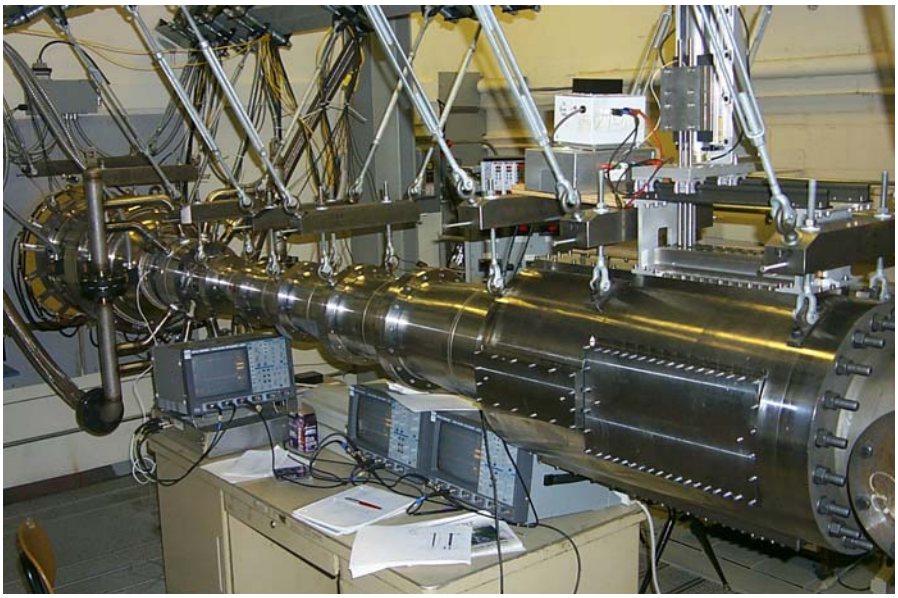

Figure 2 – Nozzle section of the Purdue Mach-6 Quiet Flow Ludwieg Tube.

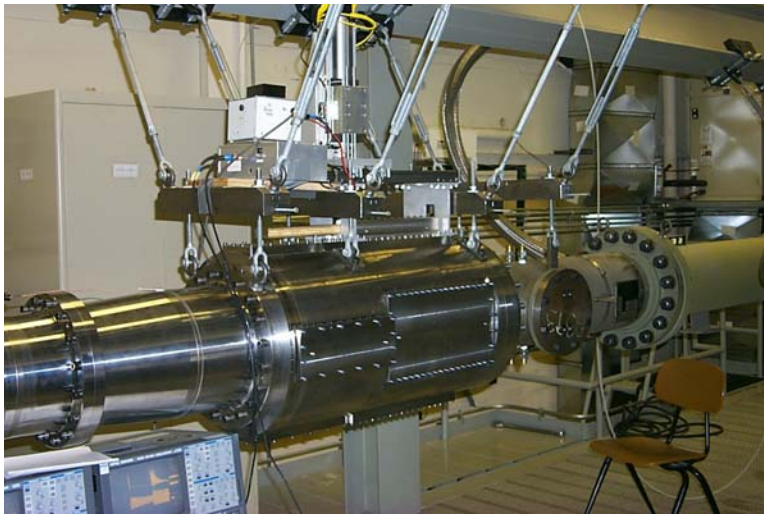

Figure 3 – Test and diffuser sections of the Purdue Mach-6 Quiet Flow Ludwieg Tube.

Figure 4 – Driver Tube of the Mach-6 tunnel.

Because of the short run time and the thin boundary layer of the models, hot wires were used to measure the parameters of the flow in the tunnel, as they are small and have a very rapid response time. The hot wires were used to study hypersonic boundary layer transition for blunt and sharp cones at various angles of attack. The position of the hot wires in the tunnel is controlled through the use of a traverse located on the upper wall of the test section, near the section of the tunnel in Figure 5 labeled "windows". In order to obtain accurate data with the hot wires, they were first calibrated under conditions similar to those expected in the Mach-6 tunnel.

Until the last year, the Purdue Mach-6 tunnel achieved quiet flow only at very low pressures (up to approximately 8 psia), where quiet flow is defined as pitot fluctuations less than 0.1% RMS [16]. The highly polished stainless steel nozzle was replaced with an unpolished aluminum nozzle so tunnel performance issues could be studied. After several runs in the tunnel, it was determined that the aluminum nozzle allowed for quiet flow up to pressures of 20 psia. The aluminum nozzle was then polished and cleaned and has since reached quiet pressures up to 130 psia, though the exact upper limit is yet unknown and has varied greatly between runs [17].

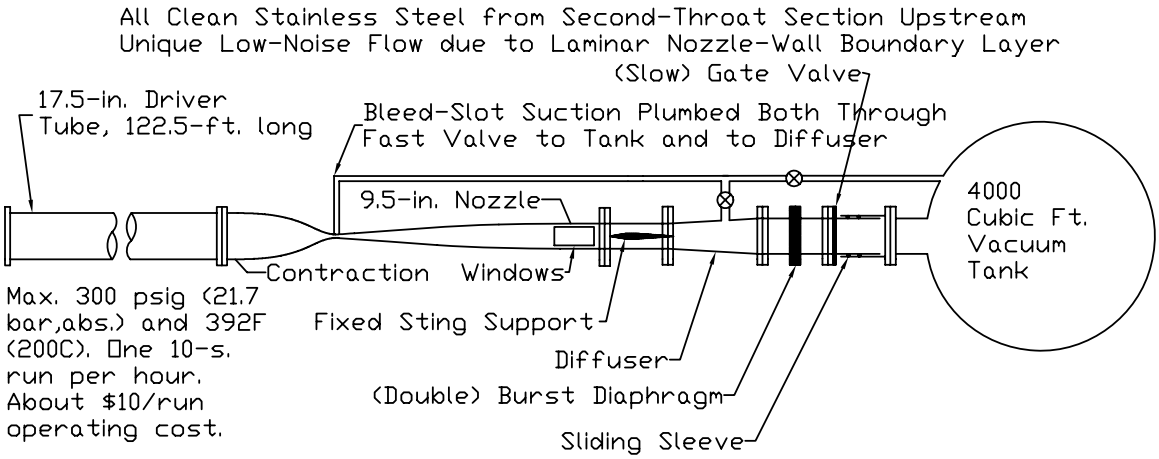

Figure 5 - Schematic of the Mach-6 Purdue Quiet-Flow Ludwieg Tube

HOT WIRE MEASUREMENTS ON SHARP CONES

Hot wire measurements were conducted to study the effect of axial location upon the instability waves on a 7° half-angle sharp cone at zero angle of attack. The cone is approximately 22.4 inches in length, has a base diameter of 5.5 inches, and a nosetip radius of 0.0025 inches. The first set of measurements was obtained using hot wire X (hwX) which has a cold resistance of approximately 12.56 Ω. This wire is Pt-10%Rh with a diameter of 0.00015 inches and a length to diameter ratio of approximately 154. The hot wire was placed 11.75, 14.0, and 16.7 inches axially downstream from the tip of the cone. This axial location of the hot wire is defined as z. An illustration of the hot wire near the cone wall is shown in Figure 6. A TSI-IFA 100 constant temperature anemometer was used with the 1:1 bridge and the overheat ratio was set to near 1.8, based on resistances. The square wave frequency response was 210 kHz, as measured in still air at ambient pressure. The driver temperature was set to 433K for these runs and the dew point measured using a Panametrics Moisture Target Series 5 Analyzer for these runs (and all other runs) was normally in the range of -25 to -30°C.

Figure 6 – Hot wire located near the cone wall in the test section of the Purdue Mach-6 Ludwieg Tube.

To avoid electrical noise from the traverse motor, each run consisted of one height above the cone wall with the hot wire placed at 1.0 mm above the cone wall for the first of these runs. These distances were measured using an Infinity Model K2 long-distance microscope with a CF-1B objective lens. An additional set of lenses is used to correct for distortion caused by the curvature of the thick Plexiglas window**.** After each run the traverse motor was engaged and the hot wire moved further away from the cone wall. The data was sampled at 1 MHz for 2 seconds (13 bit resolution) using a Tektronix TDS7104 digital oscilloscope in Hi-Res mode (TDS7000 Manual). In Hi-Res mode, data is sampled at 1 GHz and averaged on the fly into memory at the sampling rate. This mode provides additional resolution and digital filtering, both important for some of the data presented. All data were analyzed for the same time-step during the run, 0.40 to 0.45 seconds.

Figure 7 is an example of the boundary layer profile obtained from the runs conducted with the hot wire located 11.75 inches aft of the nosetip and an initial driver pressure of 90 psia. As illustrated in Figure 7, the mean voltage increases as the hot wire is moved away from the wall until a maximum value is reached, between 1.75 and 2.0 mm, which indicates the edge of the boundary layer. The value of the mean voltage outside of the boundary layer is relatively constant.

Mass flux was calculated from the output voltage of the CTA using the calibration curves for this particular wire. A comparison of the mass flux calculated from the hot wire measurements on the cone with the mass flux calculated by Robarge [1] using STABL is shown in Figure 8. The boundary layer thickness found experimentally is very similar to that found computationally; however, the mass flux values found far outside the edge of the boundary layer were found to be approximately 10% higher then the computational values. This discrepancy is most likely due to the extrapolation used in the calibration curves at lower Reynolds numbers. The current calibration rig does not cover the full range of Reynolds numbers seen in the Mach-6 tunnel and extrapolation of the data is used to extend the calibration curve to lower Reynolds numbers.

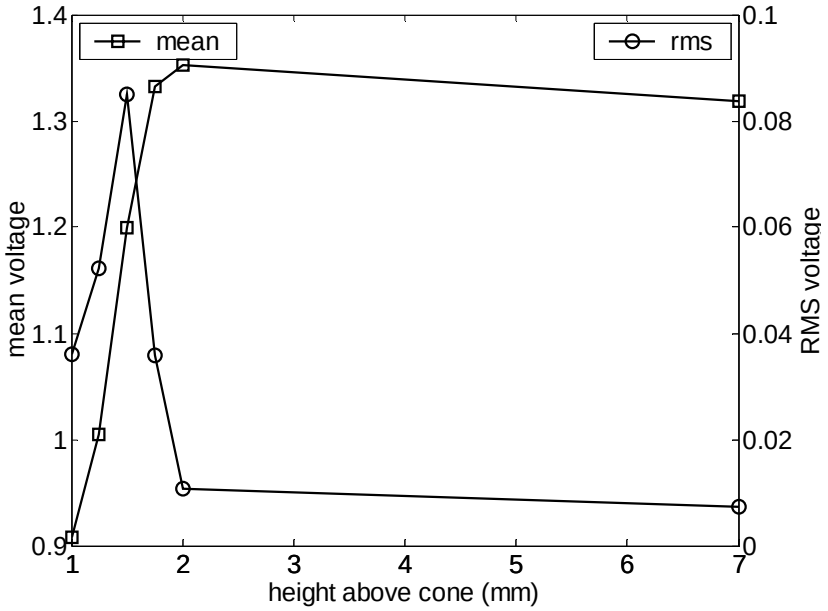

Figure 7 – Boundary layer profile on a sharp cone at 0° AOA, with a driver pressure of 90 psia and the hot wire located 11.75 inches aft of the nosetip.

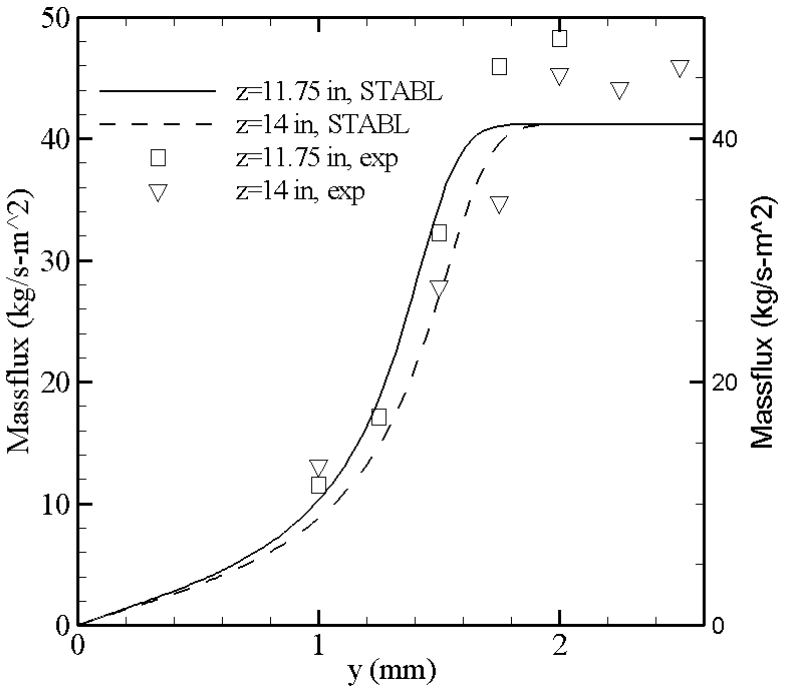

Figure 8 – Comparison of calibrated hot wire measurements on a sharp cone at 90 psia in the Purdue Mach-6 tunnel with the mass flux calculated by Robarge [1] using STABL.

Variations in the amplitudes of the hot wire fluctuations are shown as a function of the height above the cone in the power spectra of Figure 9. There appears to be an instability wave occurring near 240 kHz. This instability wave is not present near the wall, but as the distance from the wall is increased the amplitude also increases until reaching its peak at approximately 1.75 mm, near the edge of the boundary layer, as expected. Then as the height is further increased the amplitude of the wave decreases and is no longer present in the spectra obtained with the hot wire located far outside the edge of the boundary layer. The sharp spike seen at 300 kHz is present for all locations except 1.0 mm and is thought to be due to a flaw in the hot wire.

The hot wire was moved aft to approximately 14, and then 16.7 inches, and the process was repeated. Figure 10 shows a comparison between the power spectra for the three axial locations. The data plotted is from the height above the wall which is nearest the edge of the boundary layer. As seen in this figure, the amplitude of the wave increases and the frequency decreases, as expected, as the hot wire is moved further aft of the nosetip. The spectrum shown for the z=16.7 inch location indicates that laminar-turbulent transition occurred somewhere between 14 and 16.7 inches aft of the nosetip, as the instability is no longer present at 16.7 inches. This corresponds to an N-factor at transition of 4.3 to 4.7 (as calculated at 14 and 16.7 inches) according to Robarge. This is in good agreement with the N-factor of 5 found by Stetson in AEDC Tunnel-B. The slightly lower values could be attributed to higher tunnel noise in the Purdue Mach-6 tunnel, which has a smaller diameter than Tunnel-B [18].

Also included in this figure are the amplification rate curves computed by Robarge using the same initial driver pressure and temperature. The frequencies of the second-mode waves are similar for each of the axial locations. The most amplified frequencies measured experimentally are within 7% of those calculated by Robarge.

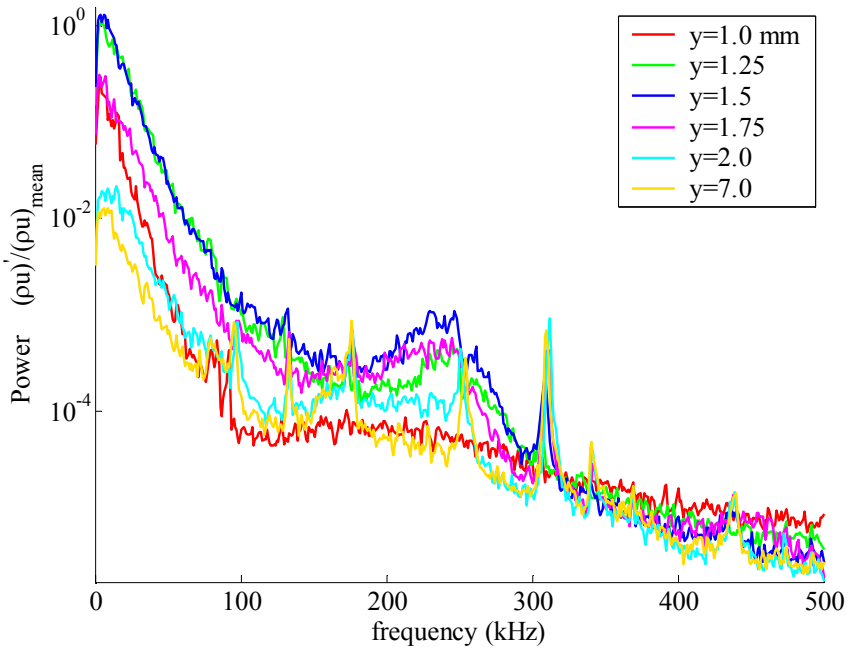

Figure 9 – Calibrated frequency spectra showing apparent second mode waves – data obtained with the hot wire located 11.75 inches aft of the nosetip on a sharp cone and 0° AOA.

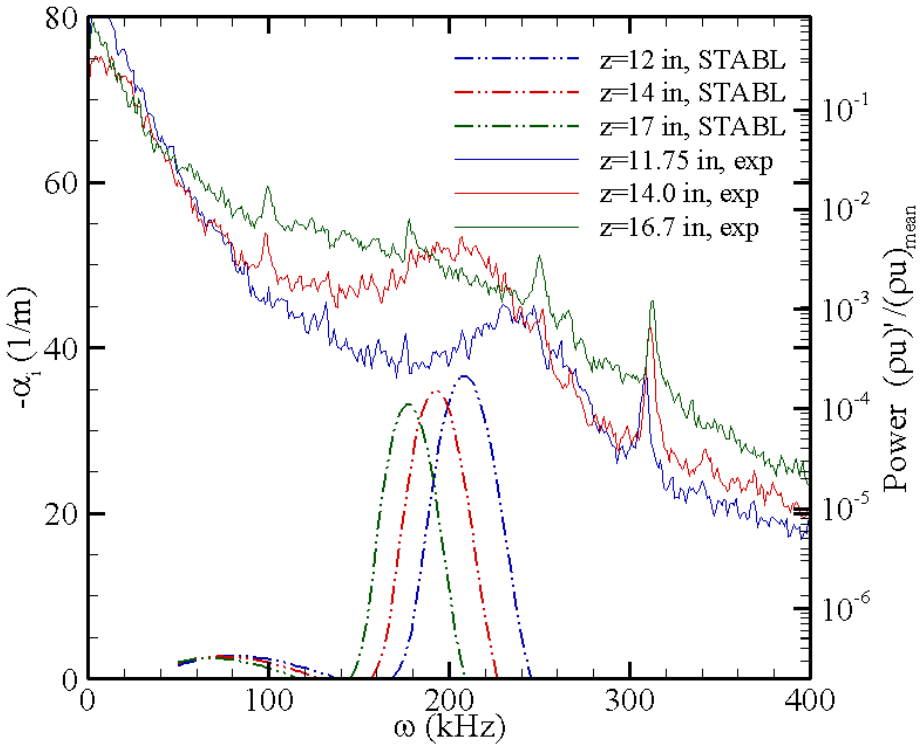

Figure 10 – Calibrated frequency spectra obtained with uncalibrated hot wires on a sharp cone at 90 psia in the Mach-6 tunnel compared to amplification rate curves for the same conditions obtained by Robarge [1] using the STABL code.

In order to better study the behavior of instability waves on sharp cones a series of data was also collected for initial driver pressures of 70 and 125 psia. The frequencies of the observed second mode instabilities along with the approximate location of transition (if one was determined) are listed in Table 1 for each of the pressures. Also listed, for the 125 and 90 psia cases, are the locally most amplified frequencies and the N-factors, at the transition location observed experimentally, as computed by Robarge. The behavior of the instabilities with both axial location and pressure were as expected, with the frequency decreasing as the distance aft of the nosetip is increased.

Table 1 – Comparison of frequencies found experimentally and as calculated by Robarge using the STABL code (most unstable frequency calculated at each location).

Pressure (psia)	Probe Location (in.)	Experiments (kHz)	STABL (kHz)	Transition Location (in.)	N_{tr}
125	10.3	280	275		>5.1
	12.3	250	245		
90	11.75	235	220	14-16.7	4.3-4.7
	14.0	200	200		
70	12.0	220	N/A	15.5-18	
	14.0	200	N/A		
	15.5	190	N/A		

HOT WIRE MEASUREMENTS ON BLUNT CONES

A 22.25 inch long blunt cone, with a 7° half-angle, was also used for testing in the Mach-6 tunnel. This cone has a 5.5 inch base diameter and a nosetip radius of 0.020 inches. The cone was placed in the test section of the tunnel at a zero angle of attack. Hot wire X, which has a cold resistance of 12.56 Ω and an aspect ratio of approximately 154, was placed at several different axial locations downstream of the nose. The overheat ratio (based on resistances) was set to 1.8 and the square wave frequency response was 210 kHz, as measured in still air at ambient pressure. Each run consisted of one height above the wall and all measurements were taken for the same time-step during the run, 0.40 to 0.45 seconds. The initial driver pressure for each run was set to 45 psia and the driver temperature to 433K.

The hot wire was originally placed 20 inches aft of the nosetip at a height of 2.0 mm above the cone. Once this first run was completed, the hot wire was moved a quarter of a millimeter further from the cone wall and second run was completed. This process was then repeated until it appeared the wire had traversed through the edge of the boundary layer. One more run was then completed with the hot wire located well outside the boundary layer. The mean and rms voltages obtained from this series of runs are shown in Figure 11. As seen in this figure, the mean voltage rises as the height of the hot wire increases until a height of approximately 3.0 mm is reached, at which point the mean voltage seems to level off. This indicates that the edge of the boundary layer on the cone is located between 2.75 and 3.0 mm above the cone wall at this axial location.

The mean voltages measured were once again converted into mass flux using the calibration curves discussed previously. The mass flux curves for both the 18 and 20 inch locations are shown as a function of height above the cone wall in Figure 12. The mass flux profiles computed by Robarge [1] under similar conditions are also shown in this figure. The shape of the profiles is very similar for each of the axial locations, though the mass flux values far outside the boundary layer found experimentally are approximately 5% less than those calculated by Robarge. Again, this difference is probably a measure of the calibration error.

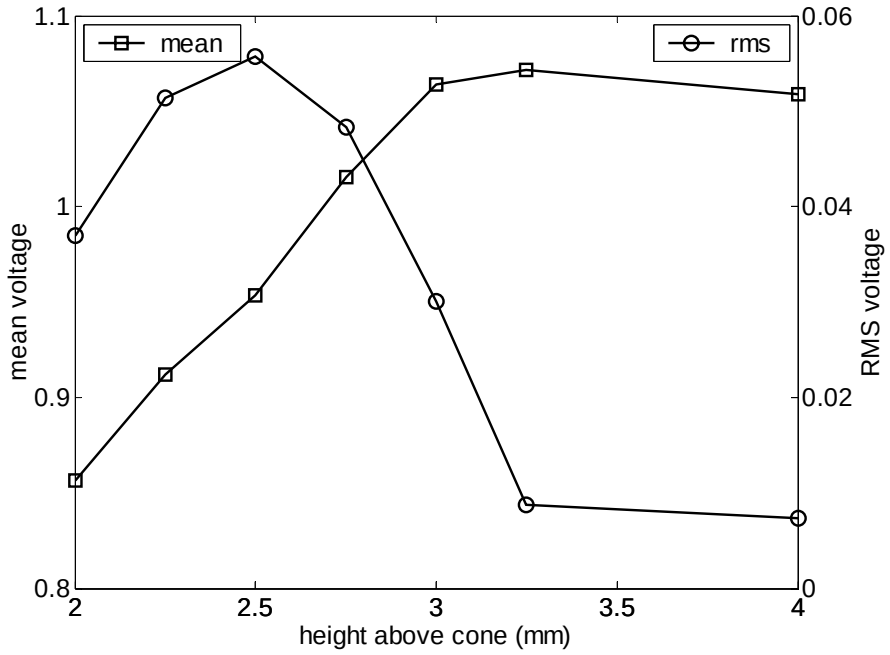

Figure 11 - Boundary layer profile on a blunt cone at 0° AOA, with a driver pressure of 45 psia and the hot wire located 20 inches aft of the nosetip.

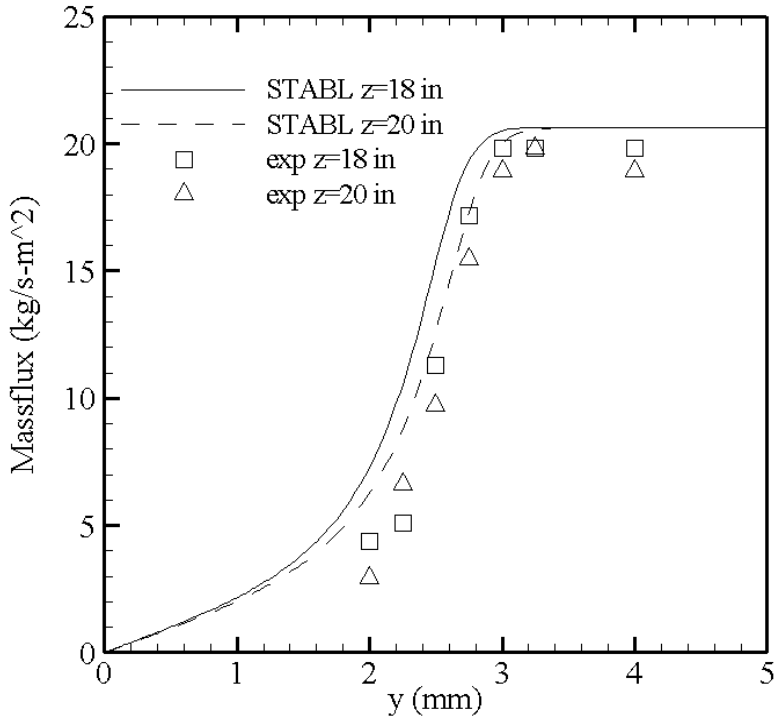

Figure 12 – Comparison of calibrated hot wire measurements on a blunt one at 45 psia in the Mach-6 tunnel with the mass flux calculated by Robarge [1] using STABL.

The variation of the instabilities as a function of height above the cone is illustrated in Figures 17 and 18. The instability occurs around 130 kHz and the amplitude increases until reaching its peak at approximately 2.75 mm. No apparent instability is present until the hot wire reaches a height of 2.25 mm above the wall. Figure 14 is a close-up of these spectra and better shows the variation of the instability with height. Again there are several sharp spikes in the spectra which are present at all heights above the cone, except those nearest the cone wall. As stated previously, these spikes are thought to be caused by a flaw in the hot wire as the frequency at which they occur is dependent on the hot-wire probe being used.

The growth of the instabilities as a function of axial location is illustrated in Figure 15. This figure shows the spectra found nearest the edge of the boundary layer (location of maximum amplitude) for three different axial locations. As seen here, when the hot wire is located 18 inches aft of the nosetip, the instability is lower in amplitude and occurs at a higher frequency then at the 20 inch location. Transition seems to occur between 20 and 22 inches aft of the nosetip, as somewhere between these locations no instability is present and the amplitude of the spectra is greater than at the two previous locations. The amplification rate curves computed by Robarge for the 18 and 20 inch location are also shown and the frequencies measured at each location are with 7% of the values computed by Robarge.

N-factors have been calculated by Robarge and the approximate location of transition, 20 to 22 inches, found experimentally corresponds to N-factors in the range of 3.6 to 4.0. This is in good agreement with the transition N-factor of 5 found by Stetson in AEDC Tunnel-B. The slightly lower values are expected, as the intensity of the tunnel noise in the Purdue Mach-6 tunnel is greater than that in Tunnel-B.

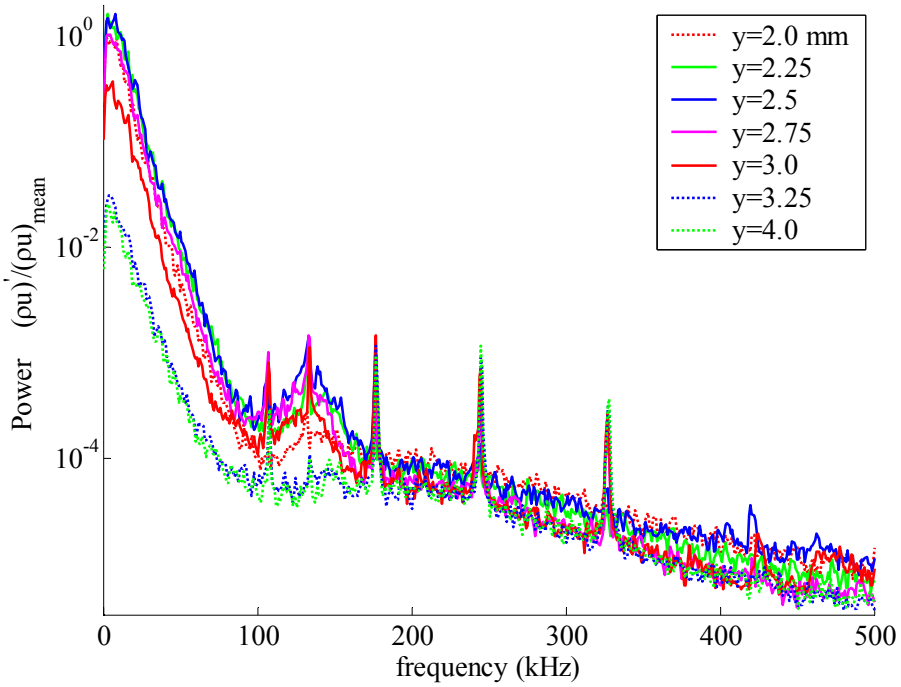

Figure 13 – Calibrated frequency spectra showing apparent second mode waves – data obtained with the hot wire located 20 inches aft of the nosetip on a bunt cone and 0° AOA.

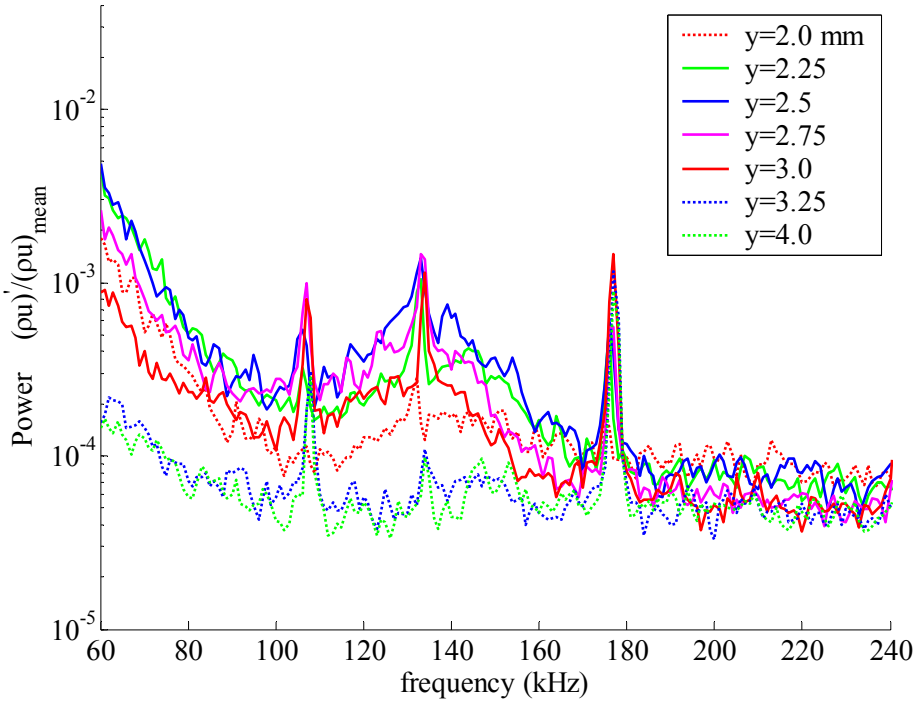

Figure 14 – Detail of the power spectra for a 7° blunt cone at zero angle of attack

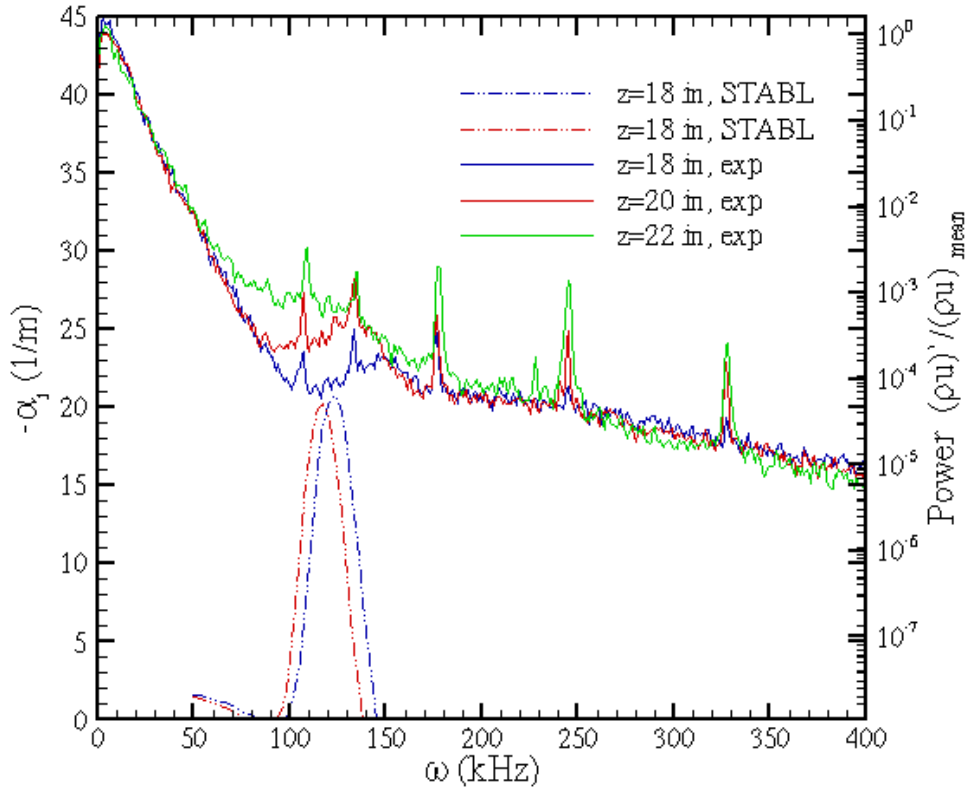

Figure 15 – Calibrated frequency spectra obtained with uncalibrated hot wires on a blunt cone at 45 psia in the Mach-6 tunnel compared to amplification rate curves for the same conditions obtained by Robarge [1] using the STABL code.

In order to better understand the behavior of instability waves on blunt cones a series of runs were also conducted at initial driver pressures of 70, 90, and 125 psia. The frequencies of the observed second mode instabilities for each of the pressures along with the approximate location of transition are listed in Table 2. Also listed on this table are the corresponding frequencies and N-factors calculated through use of the STABL code. As expected, the location of transition seems to move aft on the cone as the pressure, or Reynolds number, is decreased. The most amplified frequency also decreases with decreasing Reynolds number, as illustrated by comparing the frequency values for z~14 mm at 125, 90, and 70 psia. All frequencies are within 8% of the values calculated by Robarge [1].

Table 2 – Comparison of frequencies found experimentally and as calculated by Robarge using the STABL code (most unstable frequency calculated at each location).

Pressure (psia)	Probe Location (in.)	Experiments (kHz)	STABL (kHz)	Transition location (in.)	N_{tr}
125	14.25	240	260		>5.4
90	14.0	215	N/A	14-16	
70	14.0	195	N/A	16-18	
	16.0	175	N/A		
45	18.0	150	140	20-22	3.6-4.0
	20.0	130	130		

HOT WIRE MEASUREMENTS UNDER QUIET-FLOW CONDITIONS

Once the tunnel was able to sustain quiet-flow conditions, with pitot fluctuations of less than 0.1%, to higher pressures (greater than 80 psia), hot wires were used to measure instabilities on the sharp cone to compare with those obtained under noisy-flow conditions. The 22.4 inch long, 5.5 inch base diameter cone was determined to cause separation in the laminar boundary layer on the tunnel walls. This was detected through the use of a hot-film array placed on the lower wall of the tunnel just upstream of the model. This cone was then replaced with a shorter, 16.3 inch long cone having a 4.0 inch base diameter. Very small periods of separation were occasionally measured with this cone, typically less than one second, but the flow was attached for enough of the run to obtain relevant data.

An uncalibrated hot wire was placed 14 inches aft of the nosetip and a series of runs were completed at various heights above the cone wall to determine if any instabilities were present. The initial driver pressure and temperature were set to 90 psia and 160° C. This axial distance and pressure were chosen so that the data could be directly compared to data taken under noisy-flow conditions when instabilities were clearly present in the flow. No instabilities were observed in the spectra under these conditions. The hot wire was then moved further aft on the cone, to approximately 16.0 inches, and again no instabilities were observed. Figure 16 compares the frequency spectra at 14 inches aft and 1.75 mm above the cone wall under quiet-flow conditions, when no instabilities are present, with noisy-flow conditions, with an instability measured at 200 kHz. Also illustrated in this figure is the significant reduction in amplitude of the low frequency tunnel noise.

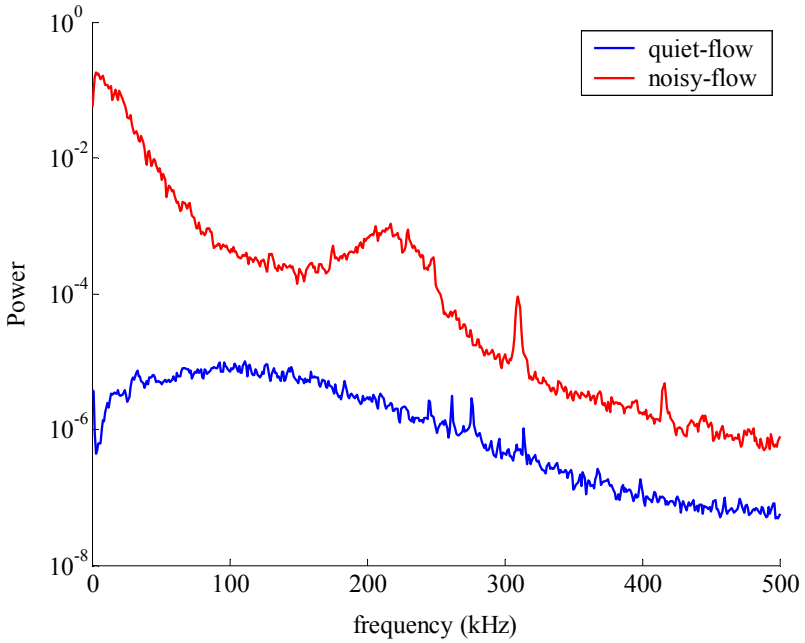

Figure 16 – Comparison of uncalibrated quiet-flow spectrum with noisy-flow spectrum at 90 psia on a 7° sharp cone at 0° angle of attack (z=14 inches, y=1.75mm).

The cone was then attached to a 3° angle of attack adapter and a series of runs were conducted to determine if the destabilization of the flow on the leeward side of the cone would allow for instabilities in the flow to be measured. The initial driver pressure for this set of runs was set to 108 psia, as that was the highest pressure at which the tunnel operated quietly. This driver pressure also allowed for a significantly longer period of attached flow than when operating the tunnel at a driver pressure of 90 psia.

The hot wire was originally placed 11.75 inches aft of the nosetip at a height of 2 mm above the cone wall. The traverse motor was turned off during the run to try and reduce the outside noise picked up in the frequency spectra. After each run the hot wire was moved 1mm until reaching a height of 7mm above the cone wall. Once the approximate edge of the boundary layer was determined a few runs where done at smaller increments near this edge to better determine the edge location. A set of data was also collected well outside the edge of the boundary layer for comparison. The boundary layer profile is illustrated in Figure 17. The mean voltage curve shows the edge of the boundary layer occurring at a height of 6.0 mm, and is corroborated by the peak in the rms voltage at the same location. As expected the boundary layer is considerably thicker than when the cone is placed at 0° angle of attack, in which case the edge of the boundary layer is observed at approximately 1.75 mm above the cone wall. Due to the quiet flow, the measured rms voltage values are close to an order of magnitude less than those measured previously.

Figure 18 shows the uncalibrated power spectra for each of the heights measured. Many seemingly random spikes are seen throughout the lower frequency portion of the spectra for each height. The cause of these spikes is unknown. The spectra for all heights other than the 5.5, 6.0, and 6.5 mm locations appear very similar in nature. At 5.5 and 6.0 mm above the cone wall it is clear that some type of instability is present as observed by the peaks in the spectra near 130 kHz as well as a smaller set of peaks occurring near 50 kHz. There is a much smaller, but still visible, peak in the spectra at 130 kHz for the height of 6.5 mm. The behavior of the peaks is similar to those observed on both the sharp and blunt cones under noisy-flow conditions. No peaks are present in the spectra near the wall of the cone or far outside the edge of the boundary layer and the largest amplitude occurs close to the measured edge of the boundary layer. This behavior would seem to indicate that these peaks are some type of instability in the flow.

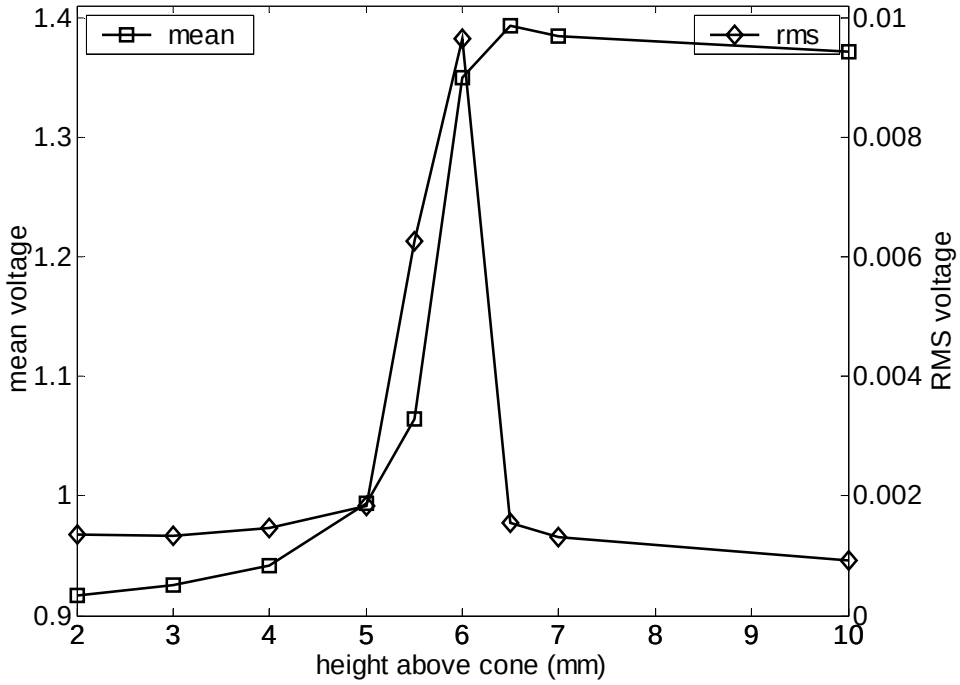

Figure 17 – Boundary layer profile of a sharp cone at 3° angle of attack and initial driver pressure of 108 psia and an axial location of 11.75 inches.

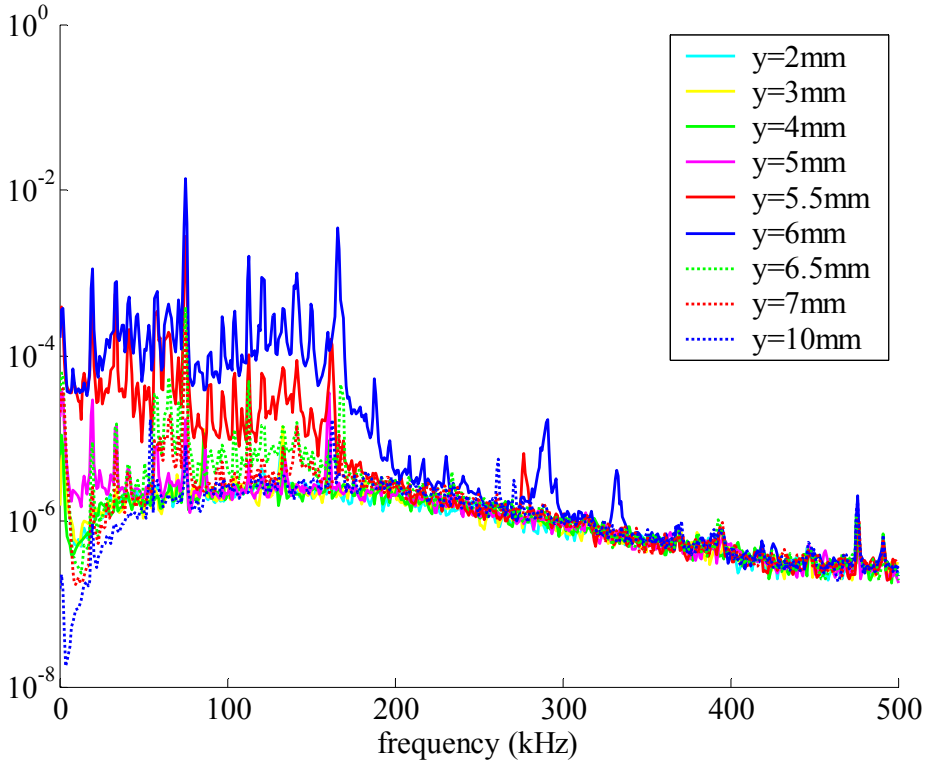

Figure 18 – Uncalibrated frequency spectra obtained on a sharp cone at 3° angle of attack and initial driver pressure of 108 psia and an axial location of 11.75 inches.

CONCLUSIONS

Several series of runs have been completed in the M-6 tunnel to study the behavior of instability waves on sharp and blunt cones. Instability waves have been visible in the power spectra obtained through the use of hot wires and exhibit expected growth patterns as the hot wires are moved axially along the length of the cone. Comparisons have been made between the experimental results and computations performed by Robarge [1] and both the boundary layer profiles and growth of the second mode instabilities exhibit similar patterns.

Due to the recent ability to achieve quiet-flow at pressure between 90 and 110 psia, measurements were obtained on the sharp cone at 0° and 3° angle of attack and were compared with those measurements taken under noisy-flow conditions. No instabilities were evident on the sharp cone at 90 psia at 0° angle of attack, when they were clearly present under the same conditions with noisy flow. However instabilities were observed on the leeward side of the cone at 3° angle of attack.

REFERENCES

[1] Robarge, Tyler. "Laminar boundary-layer instabilities on hypersonic cones: computations for benchmark experiments," Master's Thesis, School of Aeronautics and Astronautics, Purdue University, August 2005. DTIC citation ADA 437208.

[2] Kenneth F. Stetson. Comments on hypersonic boundary-layer transition. WRDC-TR-90-3057, September 1990.

[3] Steven P. Schneider. Hypersonic laminar-turbulent transition on circular cones and scramjet forebodies. *Progress in Aerospace Sciences* 40, 2004, pp 1-50.

[4] J. M. Kendall. Wind tunnel experiments relating to supersonic and hypersonic boundary layer transition. *AIAA Journal,* 13(3):290-299, 1975.

[5] Kenneth F. Stetson and Roger L. Kimmel. On hypersonic boundary layer stability. AIAA-92-0737, January 1992.

[6] M. R. Malik, R. E. Spall and C. L. Chang. Effect of nose bluntness on boundary layer stability and transition. AIAA-90-0112, January 1990.

[7] D. J. Singh, A. Kumar, and S. N. Tiwari. Effect of nose bluntness on flow field over slender bodies in hypersonic flows. AIAA-89-0270, January 1989

[8] John D. Anderson. Hypersonic and High Temperature Gas Dynamics. McGraw-Hill, Inc., New York, 1989.

[9] M. S. Holden. Leading edge bluntness and boundary layer displacement effects on attached and separated laminar boundary layers in compression corner. AIAA-68-68, 1968.

[10] Eric J. Softley. Transition of the hypersonic boundary layer on a cone: Part II – Experiments at M=10 and more on blunt cone transition. Space Sciences Laboratory, R68SD14, October 1968.

[11] I. S. Rosenboom, S. Hein, and U. Dallmann. Influence of nose bluntness on boundary-layer instabilities in hypersonic cone flows. AIAA-99-3591, 1999.

[12] K. F. Stetson, E. R. Thompson, J. C. Donaldson, and L. G. Siler. Laminar boundary layer stability experiments on a cone at Mach 8, Part 2: Blunt cone. AIAA-84-0006, January 1984.

[13] W. L. Hankey, and M. S. Holden. Two-dimensional shock wave-boundary layer interactions in high speed flows. AGARDograph 203, AGARD, June 1975.

[14] James F. Muir and Amado A. Trujillo, "Experimental investigation of the effects of nose bluntness, free-stream unit Reynolds number, and angle of attack on cone boundary layer transition at a Mach number of 6," AIAA-72-216, January 1972.

[15] K.F. Stetson, E.R. Thompson, J.C. Donaldson, and L.G. Siler, "Laminar boundary layer stability experiments on a cone at Mach 8, Part 3: Sharp cone at angle of attack," AIAA-85-0492, January 1985.

[16] Steven P. Schneider, "Effects of high-speed tunnel noise on laminar-turbulent transition," *Journal of Spacecraft and Rockets*, 38(3)323-333, May-June 2001.

[17] Steven P. Schneider, Thomas J. Juliano, and Matthew P. Borg, "High-Reynolds-Number Laminar Flow in the Mach-6 Quiet-Flow Ludwieg Tube" AIAA 2006-3056, June 2006.

[18] Schneider, Steven P. and Craig Skoch, "Mean Flow and Noise Measurements in the Purdue Mach-6 Quiet-Flow Ludwieg Tube," AIAA 2001-2778, June 2001.